The Role of Disk Tearing and Precession in the Observed Variability of Pleione

K. C. MARR,[1] C. E. JONES,[1] C. TYCNER,[2] A. C. CARCIOFI,[3] AND A. C. FONSECA SILVA[3]

[1]*Department of Physics and Astronomy, University of Western Ontario, London, ON N6A 3K7, Canada*
[2]*Department of Physics, Central Michigan University, Mount Pleasant, MI 48859.*
[3]*Instituto de Astronomia, Geofísica e Ciências Atmosféricas, Universidade de São Paulo, Rua do Matão 1226, Cidade Universitária, 05508-900 São Paulo, SP, Brazil*

Submitted to ApJ

ABSTRACT

We acquired Hα spectroscopic observations from 2005 to 2019 showing Pleione has transitioned from a Be phase to a Be-shell phase during this period. Using the radiative transfer code HDUST we created a grid of $\sim 100,000$ disk models for Pleione. We successfully reproduced the observed transition with a disk model that varies in inclination while maintaining an equatorial density of $\rho_0(r) = 3 \times 10^{-11}(r/R_{eq})^{-2.7}$ g cm^{-3}, and an Hα emitting region extending to 15 R$_{eq}$. We use a precessing disk model to extrapolate the changing disk inclination over 120 years and follow the variability in archival observations. The best-fit disk model precesses over a line of sight inclination between $\sim 25°$ and $\sim 144°$ with a precessional period of ~ 80.5 years. Our precessing models match some of the observed variability but fail to reproduce all of the historical data available. Therefore, we propose an ad-hoc model based on our precessing disk model inspired by recent SPH simulations of similar systems, where the disk tears due to the tidal influence of a companion star. In this model, a single disk is slowly tilted to an angle of 30° from the stellar equator over 34 years. Then, the disk is torn by the companion's tidal torque, with the outer region separating from the innermost disk. The small inner disk returns to the stellar equator as mass injection remains constant. The outer disk precesses for ~ 15 years before gradually dissipating. The process repeats every 34 years and reproduces all trends in Pleione's variability.

Keywords: stars: early-type – stars: emission-line, Be – stars: individual: 28 Tau

1. INTRODUCTION

Over the past 130 years, the Be star Pleione (HD23862, 28 Tau) has exhibited remarkable spectroscopic and photometric variations. Frost (1906) first realized the extreme nature of its variability in 1905 and 1906 when he discovered that its previously bright emission lines had disappeared in only a few years. Since this time, Pleione's hydrogen and metal line profiles have exhibited a wide range of shapes, including absorption lines (diskless phase) (McLaughlin 1938), doubly-peaked emission lines (Be phase) (Doazan & Underhill 1986) and emission with narrow absorption cores (Be-shell phase) (Delplace & Hubert 1973). The reader can find a historical account of the changes in Pleione's spectrum by Gulliver (1977) and Hirata (1995), with recent activity described by Nemravová et al. (2010).

The spectral type of B8 Vpe for Pleione was first determined by observations taken during a diskless phase

by Lindblad (1922), and was later confirmed by Frost et al. (1926) and Merrill & Burwell (1933). Other details about this system, such as the nature of its companion stars and the interpretation of its variability are much less clear. Katahira et al. (1996a,b) found the near companion to have a 218 day orbital period with an eccentricity of 0.6 by analyzing the variation of radial velocities in Hα emission from two consecutive shell phases. By similar means, Nemravová et al. (2010) confirmed the 218 day orbit and found that the eccentricity is likely > 0.7. The inclination angle of the companion's orbital plane has not been reported in the literature.

Long-term variability has also been observed in Pleione since the end of its last diskless phase in 1937. Since then, its Balmer emission lines have continuously transitioned between Be and Be-shell phases with a ~ 34 year period (Katahira et al. 1996a; Hummel 1998). Using lunar occultation methods, Gies et al. (1990) detected asymmetry in the disk that was consistent with

previously known long-term V/R variability, and speculated that the repeating Be to Be-shell phase transitions are a product of the companion's periastron passages. Iliev et al. (2007) and Iliev (2019) found that the size of the Hα and Hβ emitting regions are synchronized with the ∼ 34 year period.

The most recent transition from a Be phase to a Be-shell phase in Hα (which, hereafter, will be referred to as the Be phase and the Be-shell phase) from 2006 to 2007 has caused uncertainty about the physical conditions of Pleione's disk causing its variability. Before this transition occurred, Hirata (2007) found the polarization position angle to steadily change over long time-scales. They argued this was the result of a uniformly precessing disk that had been tilted off-axis by tidal interactions with the companion. They asserted that this model explains the repeating Be-shell to Be phase changes, with the shell lines appearing (1973) and disappearing (1988) around a disk inclination of 60°. However, their model was unable to match the rapid drop in magnitude that accompanied the 2006 to 2007 Be to Be-shell transition.

Studying the photometric and spectroscopic variability of Pleione from 2005 November to 2007 April, Tanaka et al. (2007) proposed that the precessing disk suggested by Hirata (2007) had been partially re-accreted before a new disk began building. With this two-disk model, they claim that the newly forming disk explains the formation of new components to the Hα and Hβ lines, while the old tilted disk is evidenced by the weakening Balmer line profiles at that time.

Using Hα observations spanning from 1994 August to 2009 February, Nemravová et al. (2010) argue that the changes in the spectrum cannot be attributed to disk precession, but rather result from physical changes to the disk's structure. Their assertion is that the full width at half maximum (FWHM) of the Hα line should increase as the precessing disk becomes more highly inclined. However, they find the FWHM of their Hα observations decreases over for a period of 15 years before the recent Be to Be-shell transition occurred, which they believe indicates physical changes to the circumstellar disk instead of a geometrical effect such as disk precession. Between 2006 and 2007 the FWHM of their Hα observations rapidly increased, and they suggest that a new disk has formed.

The goal of this work is to find a Be star disk model that describes the physical and geometrical state of Pleione's disk and evaluate a precessing disk model as constrained by Hα spectra, V-band photometry and optical polarimetry. These observations are described along with archival UV through IR continuum observations, as well as photometry and Balmer series spectra
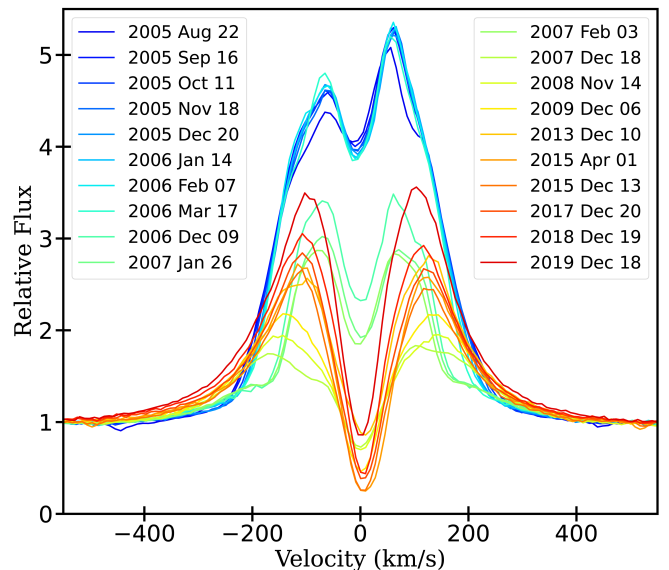
Figure 1. Hα line profile of Pleione observed at Lowell Observatory between 2005 August and 2019 December. The three epochs are differentiated by colour: the Be phase (blue), the transitioning phase (yellow), and the Be-shell phase (red).

corresponding to a diskless phase in Section 2. Section 3 outlines our method for determining the star's parameters. In Section 4, we describe our modelling procedures and the best-fit disk models. We also evaluate a precessing disk model and then propose an ad-hoc model that fits all observables based on our findings. Section 5 provides a comparison of our results with the literature and a discussion of future work.

2. OBSERVATIONS

2.1. *Spectroscopy*

2.1.1. *Be and Be-shell Phase Spectra*

Hα spectra were obtained at the Lowell Observatory, in Flagstaff, AZ, USA, using a fiber-fed echelle spectrograph connected to the 1.1 m John S. Hall telescope. The properties of the spectrograph are outlined in Hall & Lockwood (1995) and the spectroscopic reduction steps used to extract the spectra from echelle orders are described in Hall et al. (1994). We have acquired 31 spectra with this instrument from 2005 to 2019 at a resolving power of 10,000 in the Hα region. These observations are available online in a machine readable format (Table 1).

The Hα spectra shown in Figure 1 begin during Pleione's most recent Be phase in 2005 and follow the transition to a Be-shell phase in 2006 and 2007. From 2008 to 2015, the line brightened as the ratio of the peak flux over the continuum flux (F/F_c) increased from ∼ 2

to 2.5. During 2015, the system's Hα equivalent width (EW) dropped by $\sim 20\,\%$. From 2016 until our latest observations in 2019, the line profile has continued to brighten to a maximum of $F/F_c \approx 3.5$.

Table 2 summarizes the characteristics of each spectrum. In particular, the peak flux of the Hα profile was on average $F/F_c \approx 5.2$ from 2005 August to 2006 March. After the transition from the Be to Be shell phase between 2006 March and 2006 December, the peak flux had decreased to a minimum of ~ 1.8. By 2013, the peak flux increased to ~ 2.8, and, despite a small decrease in 2015, continued to increase to ~ 3.5 by 2019 December.

The violet (V) and red (R) peaks, measured as the maximum flux values within each peak, had the greatest difference during the Be phase, between 2005 August and 2006 February, with an average ratio of $V/R \approx 0.87$. Afterward, during the shell phase, the V/R ratio remained closer to unity.

The EW was relatively constant between 2005 August and 2006 March. Between 2006 March and 2006 December, during the transition from the Be to Be-shell phase, the Hα EW decreased by ~ 1.1 nm. The EW increased by ~ 0.5 nm between 2008 and 2013, and then decreased by ~ 0.3 nm by the end of 2015. Since then, the EW has increased by ~ 0.9 nm to -1.7 nm.

Archival Hα spectra of Pleione from the Be Star Spectra Database[1] were also acquired to track the change in Hα EW over time. We used 419 spectra from 2007 to 2021 observed by amateur astronomers Ernst Pollmann (Pollmann 2020) and Joan Guarro i Fló. We also used Hα EW observations from Hirata & Kogure (1976); Hirata (1995, 2007), which collectively span from 1953 to 2004. Each of these measurements are presented alongside our own for comparison to our precessing disk model in Section 4.

We obtained 70 ultraviolet (UV) spectra, observed by the International Ultraviolet Explorer (IUE) between 1979 July and 1995 March, from the INES database (González-Riestra et al. 2001) following the selection procedure described by Freire Ferrero et al. (2012). These observations were taken with the large aperture and high dispersion settings on both the short-wavelength (1,150 – 2,000 Å) and long-wavelength (1,850 – 3,300 Å) spectrographs to ensure proper flux calibration and a high spectral resolution of approximately 0.2 Å (ESA 2000). We chose to remove the IUE data beyond 0.3 μm due to instrumental limitations that cause significant uncertainty (González-Riestra et al. 2001). Figure 2 illustrates how the UV flux steadily

---

[1] http://basebe.obspm.fr/basebe/

Table 1. Hα observations of Pleione from the Lowell Observatory. The 31 spectra are identified chronologically by spectrum ID number. The full table is available online in machine-readable form.

Spectrum ID Number	MJD (+2400000.5)	λ [nm]	F/F_c
1	53604	648.183655	1.005251
1	53604	648.207947	1.036522
1	53604	648.232300	0.971167
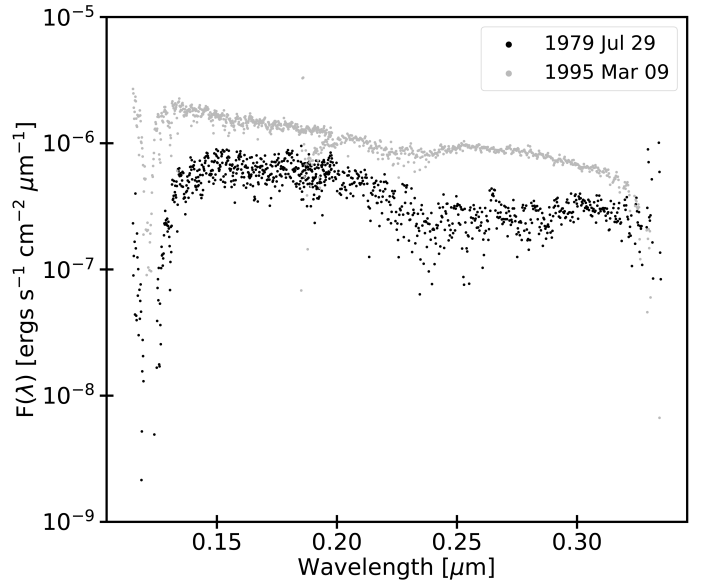
Figure 2. Upper and lower limits of the variable UV continuum observed by the IUE.

increased by a factor of ~ 3 to 4 during the time-frame of the IUE observations. How this affects our determination of the stellar parameters is discussed in Section 3

2.1.2. *Digitization of Diskless Spectra*

We acquired four Balmer series spectra of Pleione during its last diskless phase (1906 to 1938 (Frost 1906; McLaughlin 1938)) from the Harvard Astronomical Plate Collection. These spectra were recorded on photographic plates in 1927 at the Cambridge Observatory, and contain only photospheric flux unaffected by the presence of a circumstellar disk. These spectra were obtained using low-resolution dispersion objective prisms on a 24-inch Clark reflector, with a 0.6 m aperture at a scale of 59.6 arcsec/mm. These photographic plates were previously unavailable in a digital format.

High-resolution photographs were taken of the emulsion side of plates designated as H02957, H02958, and

Table 2. Hα emission line profile characteristics of Pleione.

Date	MJD (+2400000.5)	EW [nm]	Peak Flux	V/R Ratio
2005 Aug 22	53604	-2.571	5.081	0.861
2005 Sep 16	53629	-2.691	5.296	0.867
2005 Sep 17	53630	-2.691	5.353	0.850
2005 Oct 11	53654	-2.658	5.291	0.871
2005 Nov 18	53692	-2.619	5.298	0.871
2005 Dec 20	53724	-2.620	5.215	0.896
2006 Jan 14	53749	-2.630	5.308	0.878
2006 Jan 24	53759	-2.562	5.122	0.874
2006 Feb 07	53773	-2.650	5.355	0.871
2006 Mar 17	53811	-2.563	5.198	0.924
2006 Dec 09	54078	-1.458	3.484	0.979
2007 Jan 26	54126	-1.209	3.021	1.050
2007 Feb 03	54134	-1.160	2.870	1.012
2007 Dec 18	54452	-0.621	1.833	0.952
2008 Nov 14	54784	-0.676	1.955	0.994
2008 Nov 15	54785	-0.704	1.985	0.985
2008 Nov 15	54785	-0.663	1.952	0.996
2009 Dec 06	54994	-0.825	2.180	1.005
2013 Dec 10	56636	-1.174	2.804	0.916
2013 Dec 10	56636	-1.194	2.811	0.913
2013 Dec 11	56637	-1.160	2.824	0.900
2015 Apr 01	57113	-0.941	2.725	1.052
2015 Apr 01	57113	-0.928	2.721	1.055
2015 Dec 13	57369	-0.860	2.656	1.083
2015 Dec 14	57370	-0.862	2.661	1.084
2017 Dec 20	58107	-1.097	2.842	1.064
2017 Dec 20	58107	-1.100	2.854	1.067
2017 Dec 20	58107	-1.097	2.854	1.072
2017 Dec 21	58108	-1.082	2.843	1.070
2018 Dec 19	58471	-1.325	3.053	1.044
2018 Dec 20	58472	-1.381	3.132	1.058
2019 Dec 18	58835	-1.748	3.560	0.982
2019 Dec 18	58835	-1.795	3.582	0.982
2019 Dec 19	58836	-1.723	3.517	0.986
2019 Dec 19	58836	-1.718	3.506	0.991

Table 3. Stellar log of observations that contained diskless spectra of Pleione.

Date	Plate Designation	Exposure Number	Prism	Exp. Time [min]
1927 Sep 26	0	H02957	D	3
1927 Sep 26	1	H02957	D	3
1927 Sep 27	1	H02958	6°	4
1927 Sep 27	1	H02959	6°	4
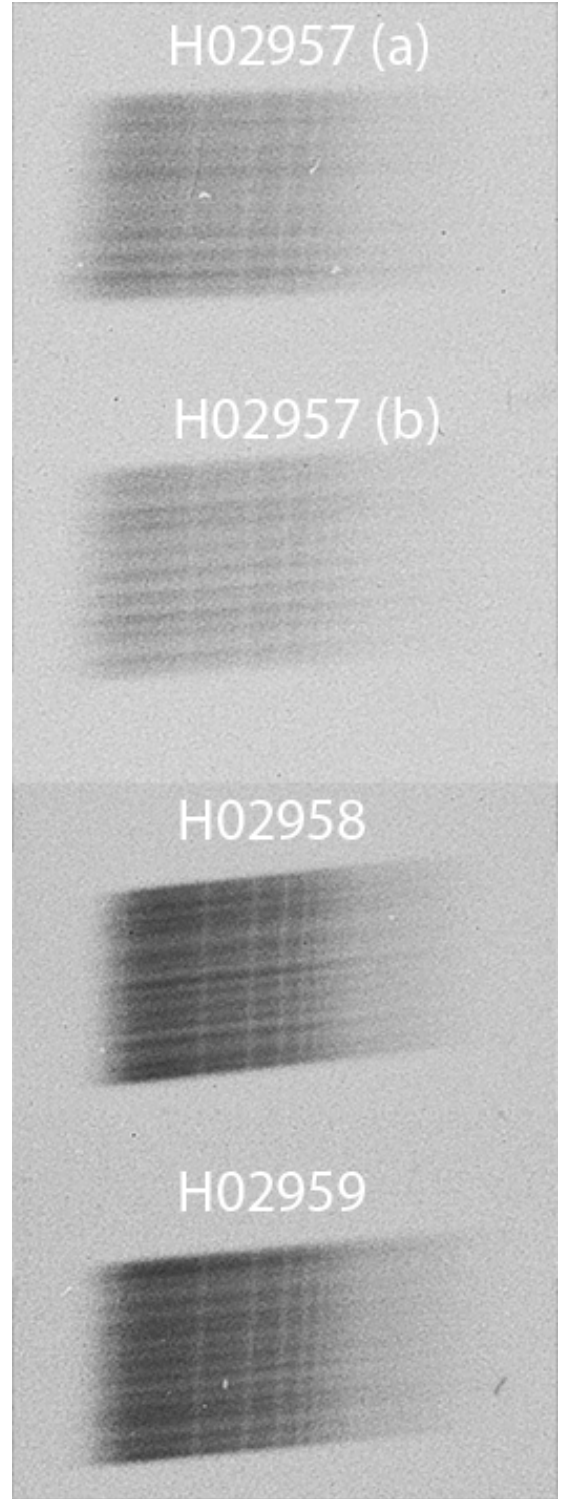
Figure 3. Photographs of Balmer series observations of Pleione taken on photographic plates in 1927 at the Cambridge Observatory. Each spectrum contains Hα, Hβ, Hγ, and Hδ lines in order from left to right. These line profiles were obtained during Pleione's last diskless phase. The plates are labelled for each spectrum by their designation in the Harvard Astronomical Plate Collection.
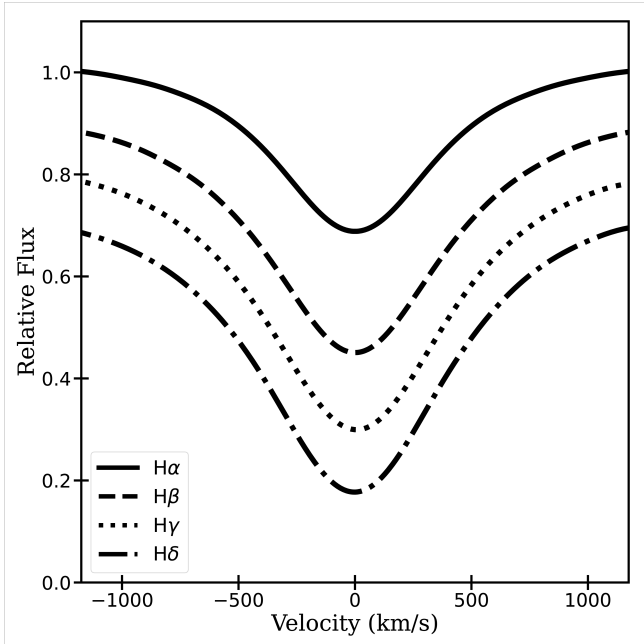
Figure 4. Hydrogen Balmer series line profiles digitized from photographic observations shown in Figure 3. These line profiles are an average of the matching profiles across each of the four photographic plate spectra. The process used for combining the different exposures of the observed spectra allows for high signal-to-noise ratio, leaving relatively little noise in the line profiles. The flux of the Hβ, Hγ and Hδ lines has been offset for ease of viewing.

H02959, according to classification system of the Harvard Astronomical Plate Collection. Figure 3 shows the averaged spectra acquired from each plate, with two spectra labelled (a) and (b) coming from plate H02957. Table 3 provides the observational details for each plate.

The spectra were extracted from the photographs by the following method. After correcting for tilt on the plate, we averaged the logarithmic intensity at each wavelength across the vertical axis of the spectrum, effectively creating a time-averaged spectrum across the duration of the exposure. The spectra were wavelength-calibrated at the center of the Hα and Hδ lines, and sampled at every 1 Å from 7000 Å to 3990 Å. The Hϵ line was not included in our data set due to low signal-to-noise ratio. Figure 4 shows the final Hα, Hβ, Hγ and Hδ spectra, where each Balmer series line has been averaged across the four observations.

To acquire the relative fluxes from each photographic plate we required the non-linear response curve of each emulsion as a function of wavelength. Since the photographic plates also have other Pleiades cluster stars, we were able to extract the response curve from the star Atlas (HD 23850, 27 Tau), a B8III spectral-type star with no reports of Hα variability in the literature over the

past 100 years. Atlas lies near Pleione on the plane of the sky, and at a similar distance (387 ly for Pleione, 422 ly for Atlas, van Leeuwen 2007). The response curve was then reconstructed by equating Atlas' spectrum from each plate to a 2004 February spectrum acquired from the ELODIE archive (Moultaka et al. 2004). The spectra for Pleione were then extracted, and transformed as a function of wavelength according to the response curve. Figure 4 shows our final Hα, Hβ, Hγ and Hδ spectra which have been averaged across the four plates. We note that Atlas is brighter than Pleione (3.5 mag vs 5.0 mag in the V-band, respectively, Ducati 2002). Therefore, for our method of obtaining the fluxes, we are assuming that both stars are appropriately exposed such that the main spectral features have photographic densities in the linear part of the response curve.

2.2. *Photometry*

Pleione has been known to be photometrically variable since 1936 (Binnendijk 1949). V-band photometric observations from 1980 to 2010 were compiled from the following publications: Sharov & Lyutyi (1988); Hirata & Kogure (1976, 1977); Hopp & Witzigmann (1980); Hopp et al. (1982); Dapergolas et al. (1981); Bohme (1984, 1985, 1986); Boehme (1988); Sharov & Lyutyi (1992, 1997); Pollmann (2011); Tanaka et al. (2007). Archival observations were acquired from the Hipparcos (van Leeuwen 2007) mission and the ASAS-3 (Pojmanski 1997) telescope archive.

Visible and infrared (IR) flux observations were obtained from the CDS Portal application from the Université de Strasbourg. The observations were compiled from catalogs which listed target objects within 0.5 arcsec of Pleione's position. The catalogs included observations from 1990 to 2010, covering both the most recent Be and Be-shell phases. This data was sourced from Stauffer et al. (2007), Egan et al. (2003) and the following missions: GAIA (Gaia Collaboration et al. 2020), 2MASS (Skrutskie et al. 2006), WISE (Wright et al. 2010), AKARI (Murakami et al. 2007), IRAS (Neugebauer et al. 1984), and Spitzer (Werner et al. 2004). These observations and the V-band photometry are presented for comparison against our precessing disk model in Section 4.

Photographic magnitudes obtained during Pleione's last diskless epoch were also obtained. In 1918, Parsons (1918) reported that Pleione had a photo-visual magnitude of 5.15 mag, and a Müller and Kempf visual magnitude of 5.08 mag. In 1922, Lindblad (1922) also reported a photo-visual magnitude of 5.15 mag. These magnitudes were used along with UV spectra to constrain Pleione's stellar parameters in Section 3.

Table 4. The best-fitting stellar parameters for Pleione computed with emcee.

Best-Fit Parameters	Values	Derived Parameters	Values
M [$M_\odot$]	$4.1^{+0.2}_{-0.2}$	L [$L_\odot$]	380^{+80}_{-70}
W	$0.8^{+0.1}_{-0.1}$	$T_{\rm eff}$ [K]	14000^{+100}_{-100}
$t/t_{\rm ms}$	$0.7^{+0.1}_{-0.1}$	$\log g$	$4.0^{+0.1}_{-0.1}$
i [°]	61^{+9}_{-8}	$R_{\rm pole}$ [$R_\odot$]	$3.3^{+0.3}_{-0.3}$
d [pc]	134^{+5}_{-5}	$R_{\rm eq}$ [$R_\odot$]	$4.4^{+0.6}_{-0.5}$
$E(B-V)$	$0.09^{+0.02}_{-0.02}$	$R_{\rm eq}/R_{\rm pole}$	$1.3^{+0.1}_{-0.1}$

Table 5. The mass, critical fraction of rotation and age used for the BeAtlas grid of models.

Parameter	Grid Values
M [$M_\odot$]	$1.7, 2, 2.5, 3, 4, 5, 7, 9, 12, 15, 20$
W	$0.00, 0.33, 0.47, 0.57, 0.66, 0.74, 0.81, 0.93, 0.99$
$t/t_{\rm ms}$	$0, 0.25, 0.5, 0.75, 1, 1.01, 1.02$

2.3. Polarimetry

We acquired observations of the optical (BVRI) linear polarization from 2010 to 2021 using the IAGPOL polarimeter at the Pico dos Dias Observatory (OPD), operated by the National Astrophysical Laboratory of Brazil (LNA) in Minas Gerais, Brazil. These observations were reduced with packages developed by the BEACON group[2], and described in Magalhaes et al. (1984, 1996) and Carciofi et al. (2007).

Archival polarization data of Pleione in the V-band were acquired from Hirata (2007), who regularly observed the star from 1975 to 2004. Observations of the V-band polarization were also acquired from the archive for the Lyot Spectropolarimeter[3] and the Halfwave Spectropolarimeter (HPOL) at the University of Wisconsin-Madison Pine Bluff Observatory, which were reduced by Draper et al. (2014). Additional polarimetric observations were extracted from Hirata (2007) using the *WebPlotDigitizer* tool from Rohatgi (2020). These archival data and our observations are presented in comparison to the percent polarization and polarization position angles of our precessing disk model in our results (Section 4).

**Table 6.** Adopted stellar parameters used as priors in emcee when fitting to the BeAtlas grid.

| Parameter	Value	Reference
parallax [mas]	7.24 ± 0.13	Gaia Collaboration et al. (2020)
$v\sin(i)$ [km/s]	286 ± 16	Frémat et al. (2005)
i [°]	60 ± 10	Hirata (2007)

3. STELLAR PARAMETERS

We used IUE UV continuum observations and diskless photographic and photo-visual band photometry from Parsons (1918) and Lindblad (1922) to determine Pleione's stellar parameters using Monte Carlo methods, using the same procedure as Marr et al. (2021). We determined the stellar mass M, critical fraction of rotation W (as defined in equation 6 of Rivinius et al. 2013), age $t/t_{\rm ms}$ (where $t_{\rm ms}$ is the main sequence lifetime, and is related to the fraction of hydrogen remaining in the stellar core), inclination i, distance d, and the degree of interstellar reddening $E(B-V)$. Additional parameters, listed in Table 4, were self-consistently derived.

Overall, a grid of 770 diskless Be star model spectra, called BeAtlas (Mota 2019), were fit to the observations. The models were computed using the 3D non-LTE radiative transfer code HDUST (Carciofi & Bjorkman 2006). HDUST computes model spectra from given stellar parameters, including M and W, as well as the polar radius ($R_{\rm pole}$), luminosity (L) and gravity darkening exponent (β). The values of $R_{\rm pole}$, L and β are correlated to M and W through the stellar evolutionary models of Georgy et al. (2013). Table 5 lists the grid size and spacing. The excess flux due to interstellar reddening, $E(B - V)$, was also included as a free parameter, with its effect on the simulated spectrum being determined using the Fitzpatrick (1999) prescription.

We used the Markov Chain Monte Carlo (MCMC) routine emcee by Foreman-Mackey et al. (2013) to determine which models from the BeAtlas grid best reproduce the observed UV spectrum using HDUST. This MCMC routine was used to generate a list of stellar parameters inside pre-determined ranges that were weighted using literature values for parallax, $v \sin i$, and i (Table 6), and then the goodness of fit for each model was computed based on the fit of the resulting continuum to the observation using a $\log(\chi^2)$ likelihood function. The fitting procedure reached convergence using 30 walkers, and 50,000 steps, with a burn-in of 5,000 steps, which were chosen following the guidelines of Foreman-Mackey et al. (2013). Further details on the emcee fitting process are given in Mota (2019).
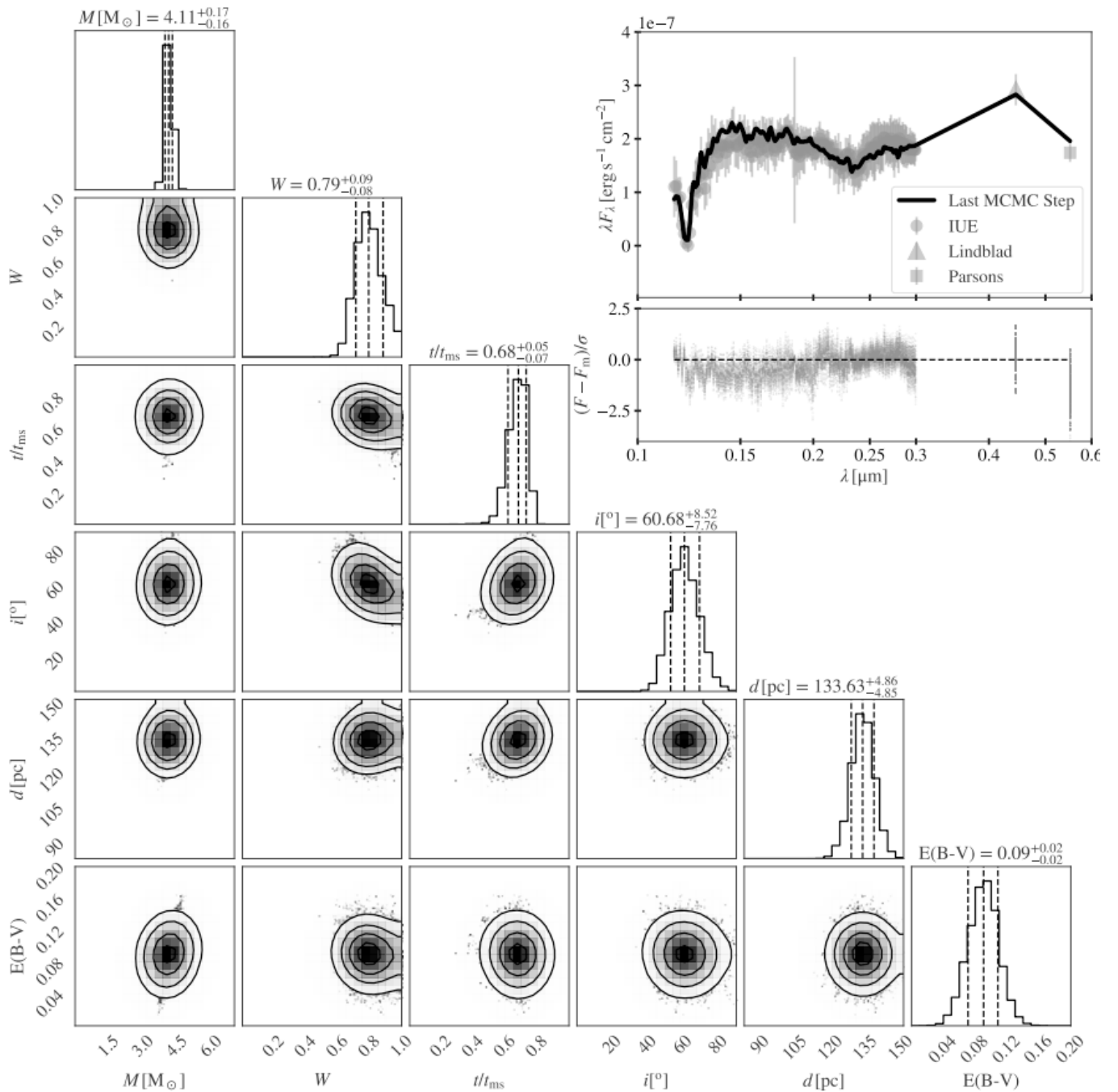
Figure 5. Best-fitting stellar parameters based on UV and visible observations of Pleione. The probability density functions of each parameter are shown on the main diagonal axis while the intersection for each parameter shows the correlation map. The six parameters used in the fitting procedure are the stellar mass M, the rotation rate W, time of life on the main sequence t/t_{ms}, stellar inclination i, distance d, and interstellar reddening $E(B - V)$. The subfigure in the top-right corner shows the most probable fit model to the UV spectra and diskless visible magnitudes, and the residuals below.
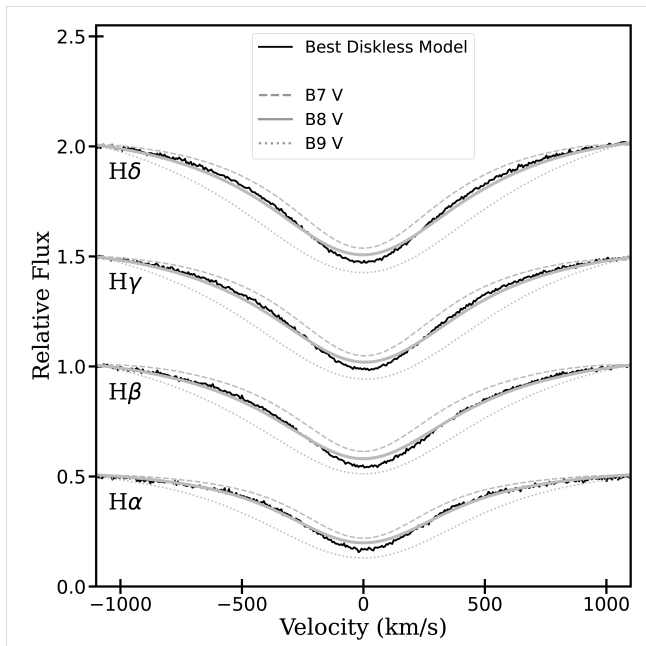
Figure 6. Hydrogen Balmer series line profiles of standard B7 V, B8 V and B9 V stars computed with HDUST using stellar parameters from Cox (2000) compared to the model lines computed using the stellar parameters in Table 4.
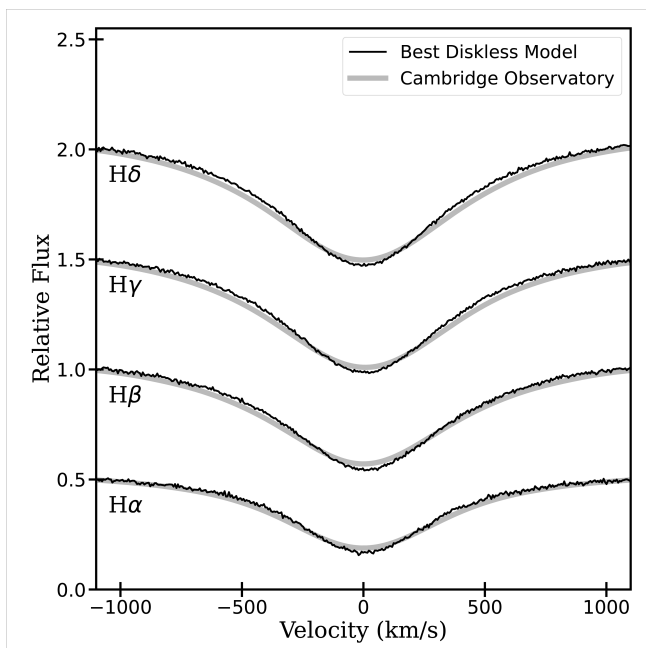
Figure 7. A comparison of Pleione's Hα, Hβ, Hγ, Hδ line profiles from 1927 (Figure 4), which correspond to the last diskless phase, with synthetic profiles computed using the best-fit stellar parameters determined with emcee and the BeAtlas grid (Table 4).

We quantified the impact of the variable UV flux on the stellar parameters by separately fitting the low (1979 July) and high (1995 March) extremes (recall Figure 2), along with the diskless visible photometry. We found M in the range 3.98 to 4.23 $M_\odot$ and $E(B-V)$ from 0.07 to 0.10 mag, while the other parameters did not change. By averaging the UV observations we find a set of stellar parameters which reproduce the UV and visible spectrum with $\chi_\nu^2 = 1.65$. The errors on these parameters include the ranges of M and $E(B-V)$ from the UV extremes.

Figure 5 depicts the stellar parameters when fitting to the averaged UV spectra and diskless visible photometry. The probability density functions (PDF) for each stellar parameter are shown along the main diagonal as histograms, and the intersections of the parameters show the corresponding correlation maps. The width of the PDF indicates how well the parameter is constrained, while the center dashed line on each histogram shows the most probable value, and the dashed lines on the left and right of center indicate the first and third quartiles. In the upper right corner of Figure 5 the SED is shown along with the best-fit model. Below the SED, the residuals between the observations and model are shown. The best-fit stellar parameters are summarized in Table 4.

As a final check of our best-fit stellar characteristics, we compared the model stellar absorption profiles to what would be expected for late B-type stars, since in the literature the spectral type of B8 V is often applied to Pleione (e.g., Gulliver 1977; Abt & Levato 1978). Specifically, we compared the synthetic hydrogen Balmer series spectra to model profiles calculated with HDUST based on standard B7 V, B8 V and B9 V star parameters from Cox (2000). Figure 6 shows our best-fit diskless model most closely resembles the B8 V hydrogen line profiles. The stellar parameters were further verified through comparison with the diskless Balmer series lines, previously described in Section 2.1.2 and Figure 7 shows the computed lines of the best-fit model overlaid with the digitized observations. We find the Hα, Hβ, Hγ, and Hδ fit the observations with $\chi_\nu^2 = 1.27$, 1.46, 1.58, 1.53, respectively.

4. DISK MODELLING

4.1. *A Precessing Disk Model*

We computed a grid of 94,720 Be star and disk models using HDUST, to model the changes observed in the Hα emission. This grid consists of axisymmetric, non-isothermal, thin-disk envelopes. The vertical disk density distributions are Gaussian, while the radial distributions follow a power-law of the form $\rho(r) \propto \rho_0 r^{-n}$,
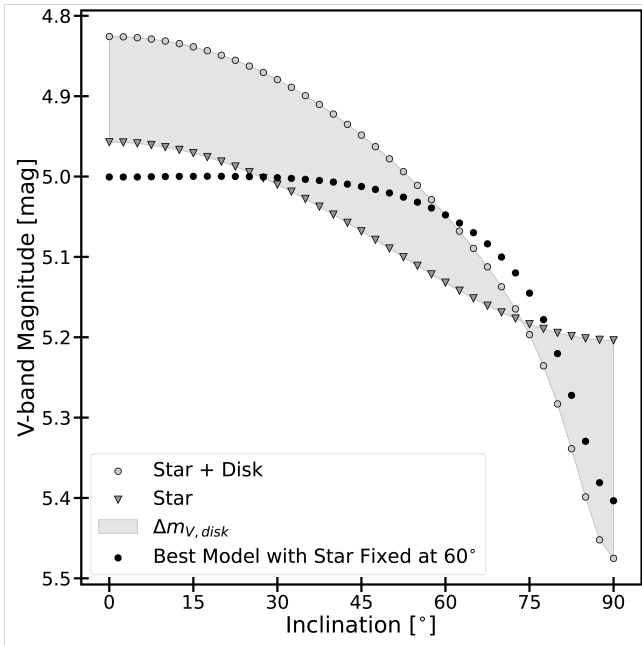
Figure 8. Change in the observed V-band apparent magnitude for different system inclinations, using the models with the best-fit stellar and disk parameters. Shown are a diskless star at different inclinations (triangles), a star and untilted disk which incline together (open circles), and a star fixed at $60°$ while the disk inclination changes (filled circles).

where ρ_0 is the density at the base of the disk ($r = R_{eq}$), and n is the density falloff exponent. Values of ρ_0 were explored in the range of 1×10^{-13} to 1×10^{-10} g cm^{-3} for every tenth of a magnitude, and the density falloff exponent n over the range of 2.0 to 3.5 in steps of 0.1. Each model was computed with the outer disk radius R_{out} at 5, 10, 15, 20, 25, 50, 75 and 100 stellar equatorial radii (R_{eq}), and using inclinations from 0 to $90°$ in steps of $2.5°$.

The line broadening effect due to non-coherent electron scattering within the disk (Auer & Mihalas 1968; Poeckert & Marlborough 1979) was approximated as it is not accounted for in HDUST simulations. For each synthetic profile, a fraction (F_e) of the synthetic Hα flux (where F_e ranged from 0.2 to 0.4) was convolved with a Gaussian of width equal to the electron velocity v_e (where v_e ranged from 400 to 800 km s^{-1}). The remaining $1 - F_e$ of the flux was left unbroadened. Through MCMC fitting with emcee, F_e and v_e were treated as free parameters within the given ranges, to determine the best possible fit for each model to the observed Hα spectra (see Marr et al. 2021, for more details on this procedure).

We find that the observed trend of the Hα profiles from 2005 to 2019 (recall Figure 1) can be reproduced by a single disk model by varying the inclination. Our

Table 7. Best-fit disk parameters obtained for each Hα line emission profile.

Date	MJD (+2400000.5)	i [$°$]	R_{out} [R_{eq}]	F_e	v_e [km s^{-1}]
2005 Aug 22	53604	30.0	15	0.34	610
2005 Sep 16	53629	32.5	15	0.35	610
2005 Sep 17	53630	32.5	15	0.35	610
2005 Oct 11	53654	32.5	15	0.35	610
2005 Nov 18	53692	32.5	15	0.35	610
2005 Dec 20	53724	32.5	15	0.35	610
2006 Jan 14	53749	32.5	15	0.35	610
2006 Jan 24	53759	32.5	15	0.35	610
2006 Feb 07	53773	32.5	15	0.35	610
2006 Mar 17	53811	32.5	15	0.35	610
2006 Dec 09	54078	35.0	15	0.30	650
2007 Jan 26	54126	35.0	15	0.33	650
2007 Feb 03	54134	35.0	15	0.31	650
2007 Dec 18	54452	37.5	15	0.25	640
2008 Nov 14	54784	40.0	15	0.25	640
2008 Nov 15	54785	40.0	15	0.24	640
2008 Nov 15	54785	40.0	15	0.24	640
2009 Dec 06	54994	42.5	15	0.28	640
2013 Dec 10	56636	60.0	15	0.30	630
2013 Dec 10	56636	60.0	15	0.30	630
2013 Dec 11	56637	60.0	15	0.30	630
2015 Apr 01	57113	65.0	15	0.29	630
2015 Apr 01	57113	65.0	15	0.29	630
2015 Dec 13	57369	65.0	15	0.29	630
2015 Dec 14	57370	65.0	15	0.29	630
2017 Dec 20	58107	75.0	15	0.31	610
2017 Dec 20	58107	75.0	15	0.31	610
2017 Dec 20	58107	75.0	15	0.31	610
2017 Dec 21	58108	75.0	15	0.31	610
2018 Dec 19	58471	77.5	15	0.33	610
2018 Dec 20	58472	77.5	15	0.33	610
2019 Dec 18	58835	80.0	15	0.35	630
2019 Dec 18	58835	80.0	15	0.35	630
2019 Dec 19	58836	80.0	15	0.35	630
2019 Dec 19	58836	80.0	15	0.35	630

models were limited to axisymmetric disks in the stellar equatorial plane, which when viewed at different inclinations require the star to be inclined at the same angle as the disk. To account for tilting, the absolute flux of the diskless model at the appropriate i was subtracted from the star and disk model at the same i to obtain flux for the inclined disk. The inclined disk flux was then added to the flux of the diskless model at $i_{star} = 60°$. We believe this first-order correction captures the most
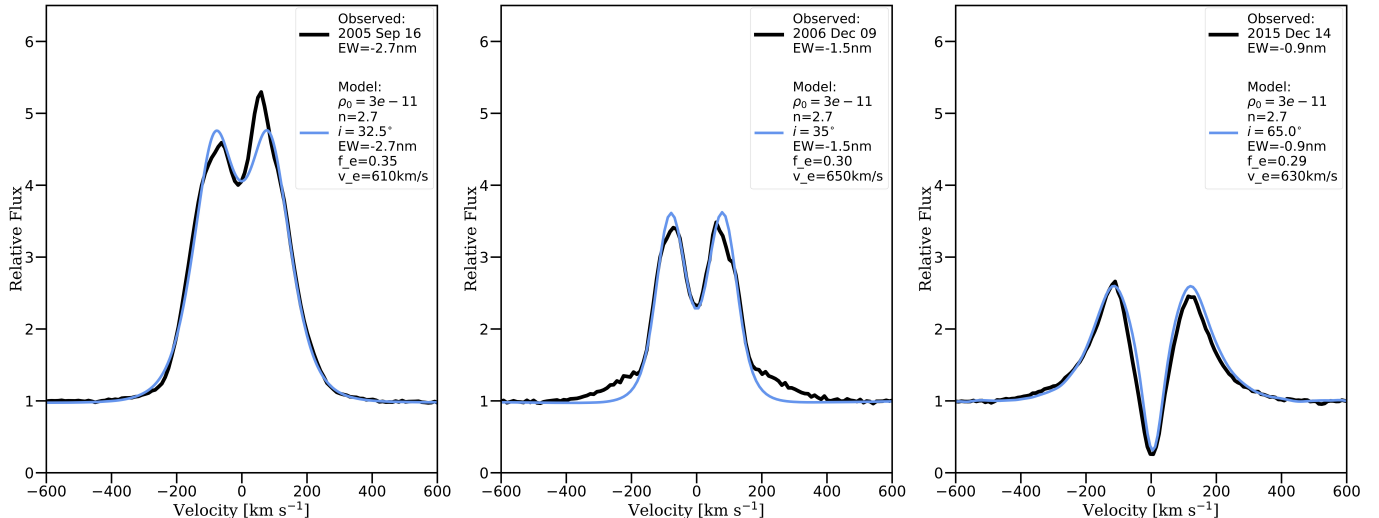
Figure 9. A comparison of the 2005 September 16 (left), 2006 December 9 (center) and 2015 December 14 (right) Hα observations from Lowell Observatory (black) to the best-fit model spectra (blue). The inclinations for the model spectra and convolving parameters are given in the legend.

significant effect on the change in flux by the tilting of the disk. This correction was applied across the entire spectrum, and affected models at low i values most. For example, at a disk inclination of $i = 0°$, correcting for the stellar component to be at $i = 60°$ (instead of $i = 0°$) caused an increase in normalized Hα peak flux of less than 40% for all models, and at $i = 30°$ the effect was less than 20%. In the V-band, this correction decreased the continuum level by ~ 0.2 mag at $i = 0°$ models, ~ 0.15 mag at $i = 30°$, and increased by ~ 0.05 at $i = 75°$ (see Figure 8).

Our best-fit model to the Hα observations has density of $\rho_0 = 3 \times 10^{-11}$ g cm^{-3} and $n = 2.7$, an outer disk radius of $R_{\rm out} = 100$ $R_{\rm eq}$, and a range of inclinations from 30° to 80°. This single density model suggests that the mass-loss rate from the star was constant during this period. We note that for the models with radii of 15 $R_{\rm eq}$ and larger, the improvements to the χ_ν^2 fit were not statistically significant. Therefore, we quote a lower limit of 15 $R_{\rm eq}$ for the Hα emitting region, while its real size remains undetermined.

Figure 9 shows a sample of three Hα profiles, chosen to illustrate how well the best-fit models match the data. The other fits to the observations that are not shown were of similar quality. The non-coherent electron scattering in the best-fit models has values of $F_e = 0.33 \pm 0.04$ and $v_e = 635 \pm 25$ km s^{-1}. This electron velocity corresponds to a temperature of ~ 8900 K, which is similar to the disk temperature of ~ 9000 K at the outer edge of the Hα emitting region given by HDUST models, and the isothermal disk temperature of ~ 8300 K (60% of T_{eff}, Carciofi & Bjorkman 2006). Our method of accounting for the broadening due to electron

scattering more strongly affects the width of Hα profiles formed at lower disk inclinations. As a result, profiles at different inclinations can have the same width, while having different strengths. The models fit with reduced χ^2 values ranging from 1.33 to 3.82. Table 7 summarizes the best-fit model disk parameters obtained from each Hα emission line observation.

During the recent Be to Be-shell transition, Pleione exhibited a rapid drop in the visible and IR continuum flux (Tanaka et al. 2007). In Figure 10, we show that our best-fit model reproduces this drop in IR flux when considering the minimum (30°) and maximum (80°) inclinations found. The best-fit model to the 2005 September 16 Hα profile fits the Be phase SED with reduced $\chi^2 = 1.93$, while the best-fit model to the 2015 December 14 observation fits the Be-shell SED with a reduced $\chi^2 = 1.65$. The UV continuum changed by less than 2% between the phases (i.e., within the error ranges). The predicted radio spectra of the simulations are shown for reference, however no radio continuum observations were available for comparison.

The inclinations of our best-fit model are shown in Figure 11 at the time of each observation. We find that over the course of our observations the disk's inclination changes at a rate of $\sim 3.7°$ per year, and was once again viewed edge-on in 2021 November.

To investigate the scenario of a precessing disk as proposed by Hirata (2007), we created a disk model by adopting equation 1 of Dunn et al. (2006), which describes the motion of a precessing galactic disk. This equation determines the inclination of the disk when provided with two values: γ, the angle between the precession axis and the observer's line of sight, and δ,
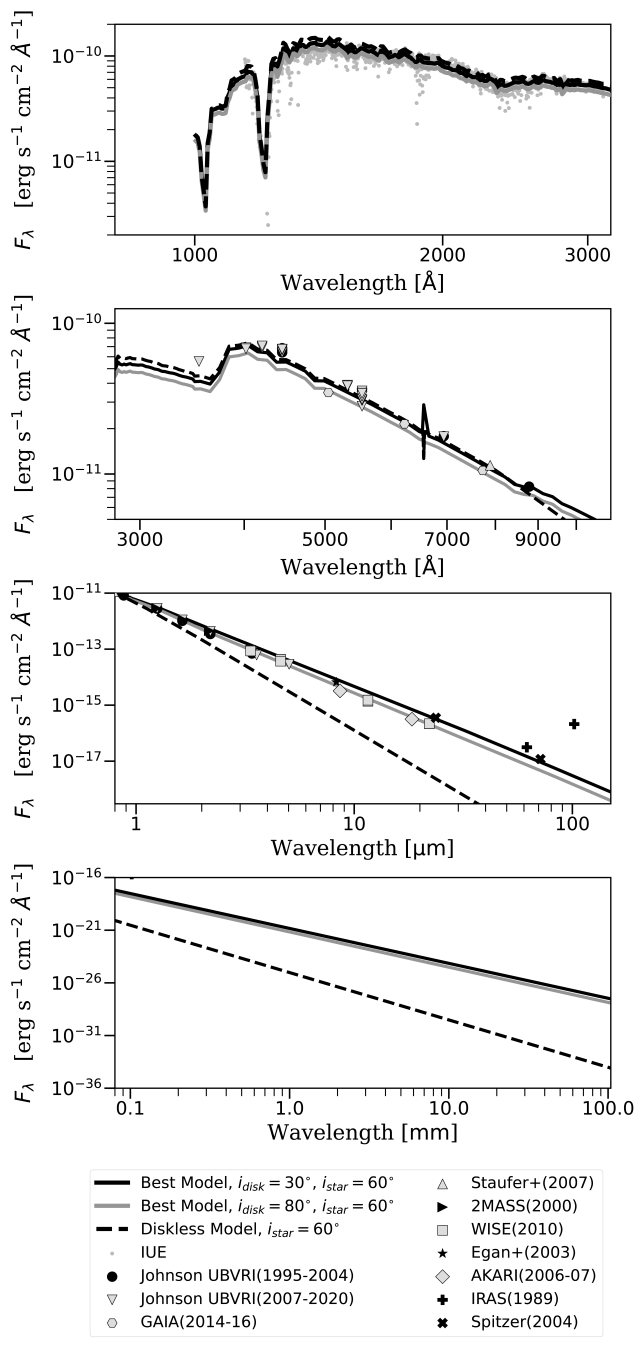
Figure 10. SED of Pleione showing the best-fit disk and diskless models in comparison to observations in the UV (top), visible (upper middle), IR (lower middle), and radio (bottom). The observations have been separated into those taken during the Be phase (black) and during the Be-shell phase (grey). The IUE observations from the Be phase are in dark grey for ease of viewing. The radio SED is shown for the best-fit disk and diskless models despite no radio observations being available for comparison.

the angle between the disk's normal and the precession axis. We used MCMC fitting with emcee to determine the values of γ and δ that best reproduced the inclinations determined through Hα fitting. We note that γ is not fixed to the stellar spin-axis. This is a reasonable assumption since the dynamical simulations of Martin et al. (2011) show that the precession axis of a misaligned circumstellar disk lies normal to the orbital plane of the companion and is not coupled to the stellar spin axis. Since we do not know the value of the orbital inclination for Pleione, it is reasonable to regard the precession axis as a free parameter. The timing of the minimum inclination and the period of the precession were also fitted parameters. We find the best-fit precession model has $\gamma = 84 \pm 3°$ and $\delta = 59 \pm 3°$, with the minimum inclination of $25°$ occurring in 2001 May, the maximum inclination of $144°$ in 2040 September, and the precession period of 29400 ± 100 days, or ~ 80.5 years. This precessing disk model is shown in Figure 11, with the grey band indicating the uncertainty. However, since only a portion of the precession period is sampled by our observed Hα profiles, the errors we find through this MCMC analysis are likely a lower bound.

The variation in Hα EW with disk inclination is shown for the precessing disk model in Figure 12. Here, the Hα EW is greatest at -2.9 Å when the disk inclination is $0°$. A secondary peak at -2.6 Å occurs around $90°$. Dramatic changes to the EW occur around particular inclinations. From $35°$ to $40°$, the EW decreases from -2.5 Å to -0.6 Å as the line transitions to a Be-shell profile. Beyond $40°$, the line has a shell profile and the peak flux increases with the inclination while also becoming narrower. At higher inclinations as the disk becomes edge-on, the stellar continuum emission falls more rapidly, resulting in increases in our normalized Hα spectra and the corresponding EW. This effect is illustrated in Figure 13. The Figure shows the Hα spectrum for different inclinations with the star fixed at $60°$, prior to normalization and the convolution process. Here, we can see the continuum flux around Hα in absolute units decreases more rapidly at high disk inclinations.

We extrapolated the precessing disk model inclinations over 120 years, from 1930 to 2050. The left side of Figure 14 shows the inclinations of the extrapolated model, along with the Hα EW, V-band photometry, V-band polarization level, and the V-band polarization position angle of our best-fit model at the inclinations of the precessing disk model (the right side of this Figure is discussed in Section 4.2). The observations previously described in Section 2 are overplotted for comparison, as well as the inclinations that Hirata (2007) derived from
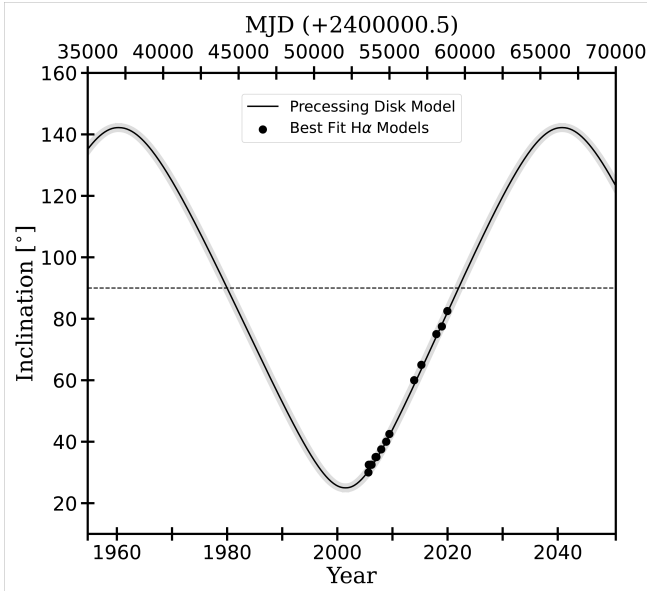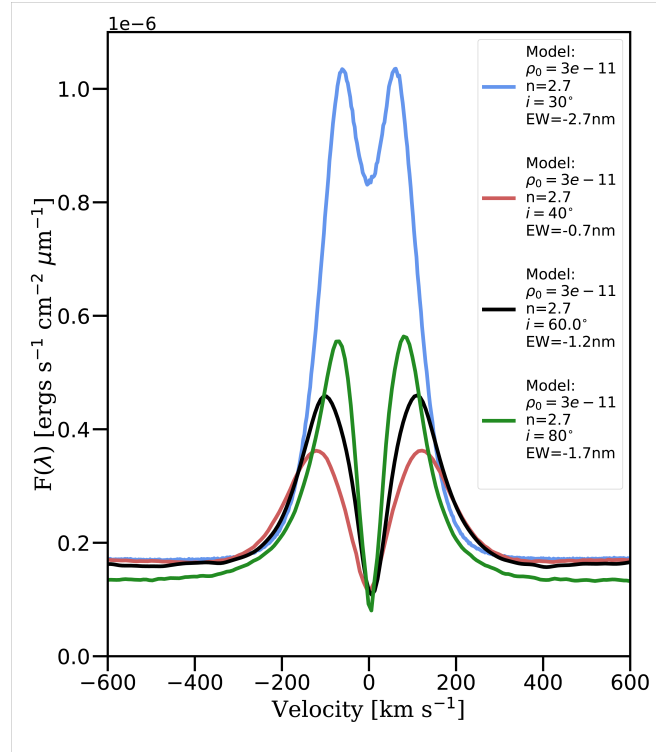
Figure 11. Change in the stellar inclination with time determined from our best-fit models to the Hα observations, along with our precessing disk model. The horizontal dashed line indicates 90° inclination. Inclinations greater than 90° occur when viewing the lower part of the disk.
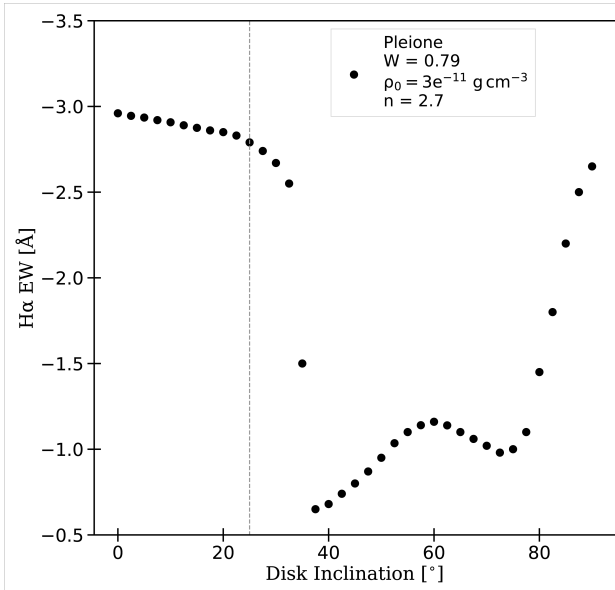
Figure 12. Variation in the EW of the Hα line profile with disk inclination, with the star fixed at 60° for our precessing disk model. All predicted inclinations from 0° to 90° are shown, however the lower limit of the inclination range determined from Hα profile fitting is indicated by the vertical dashed line.

their model. As our disk models are axisymmetric, the observables produced are symmetric about 90°.

In the second panel on the left side of Figure 14, we show the trend of the Hα EW of our precessing disk

Figure 13. Subset of the best-fit predicted Hα profiles in absolute flux units, before convolution. The stellar inclination is fixed at 60°. The disk inclinations for each model spectrum are given in the legend.

model, which is limited to the inclinations determined from the line profile fitting. As the inclination range is $> 25°$, the maximum EW observed is -2.8 Å. Note that in this Figure the grey shaded region is the same as what is shown in Figure 12 to the right of the vertical dashed line. Overall, the trends in the Hα EW, are mirrored about 90° due to the symmetry of the precessing disk.

From 2005 to 2019, the best-fit tilted disk model fits our Hα observations with reduced $\chi^2 = 1.6$. Outside of this period, our models cannot reproduce the observed trend using the ~ 80.5 year precession period. We note that while a shorter period would improve the timing of the fit to the previous Be-shell phase in the 1970's, it also would make the model progress through its Hα EW trend faster than what is observed.

In the third panel on the left side of Figure 14, we see our precessing disk model is able to reproduce the gradually increasing V-band magnitude, from 1988 to 2004. In 2004, the model reaches an average observed magnitude of ~ 5.02 mag, before the model and observations diverge in 2007 when the magnitude was observed to rapidly drop by 0.3 mag. During this time, our precessing disk model takes ~ 14 years to decline to this value. The minimum brightness of our model is ~ 5.38 mag,
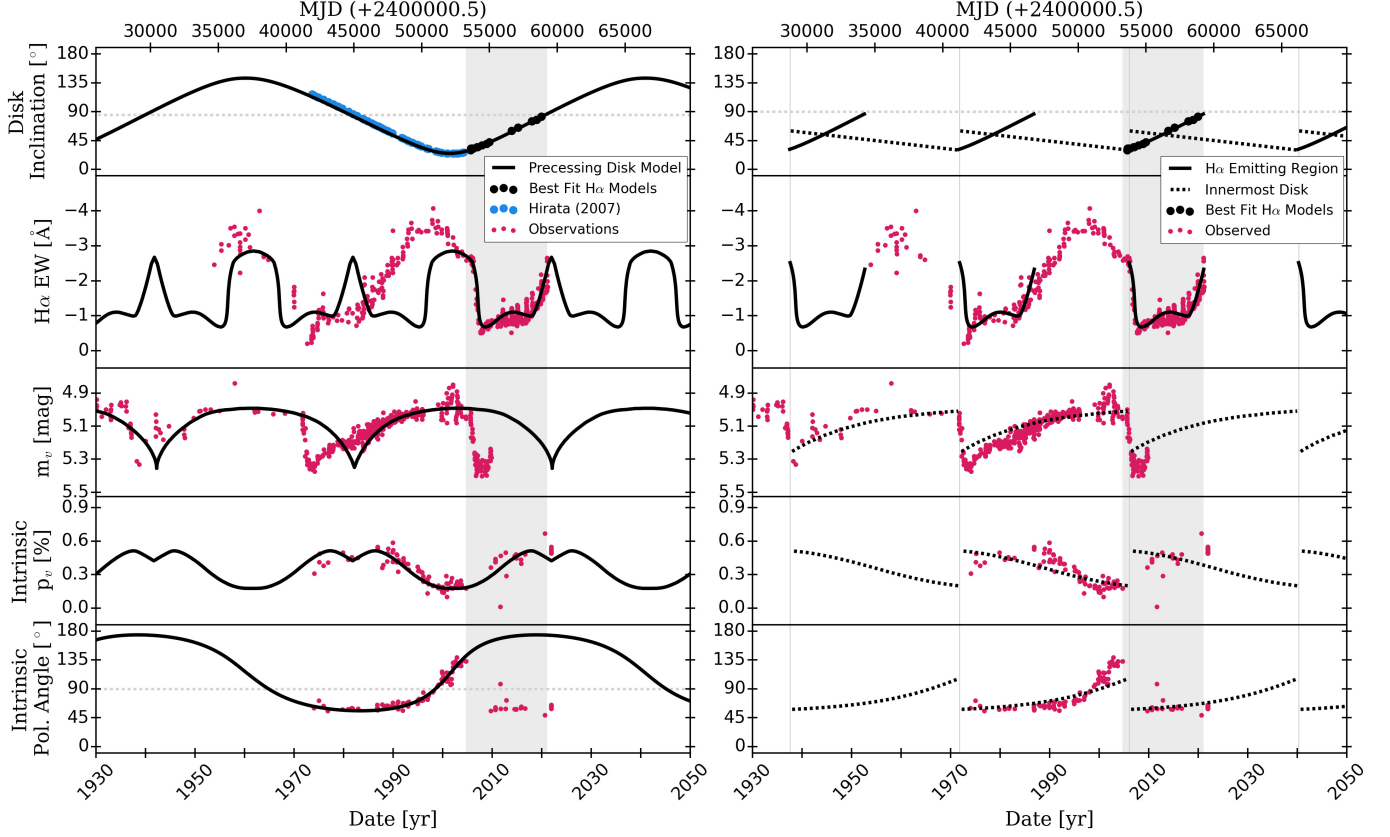
Figure 14. *Left:* Comparison of the precessing disk model (black, solid line) with an 80.5 year period to archival observations (red), and to the inclinations from Hirata (2007)'s model (blue) and from our best-fit Hα model (black). The light grey vertical band indicates the region over which our Hα observations were modelled. In the top panel, the grey horizontal dashed line shows the inclination of 83.6° that the precession is centered about. *Right:* The same as the left side but instead showing the ad-hoc disk tearing disk model. The precessing Hα emitting region (black, solid line) precesses for the first 15 years of the 34 year Be-shell to Be phase cycle. In the same period, the innermost disk (black, dotted line) gradually transitions from the stellar equator at 60° to 30°. The thin, vertical grey lines indicate each disk tearing event. Hirata (2007)'s inclinations are not included as they follow the precession of a disk in V-band polarization, not Hα emission.

which occurs in 2021. As the rapid Be to Be-shell transition occurs every ~ 34 years while half of the precession period is ~ 40 years, we see that the previous minimum in brightness occurs in 1982, just ~ 8 years after the observed minimum.

The polarization level of our best-fit model is shown in the fourth panel of the left side of Figure 14. The maximum polarization level of ~ 0.53% is observed at ~ 70°. Projecting our best-fit models forward in time along inclination curve produces the polarization signature of a tilted disk, similar to those shown in Marr et al. (2018). The polarization from the model fits the observations with reduced $\chi^2 = 1.7$.

To get the polarization position angle of our precessing disk model, we used equation 2 from Dunn et al. (2006) to first extract the angle between the precession axis of the star projected onto the sky and the normal of the disk projected onto the sky. This angle has a constant offset from the polarization position angle, which is the

angle between north on the sky and the projected precession axis of the star. We find this angle is ~ 115° to align our best-fit precession model with the observed, intrinsic polarization position angle. The bottom panel of Figure 14 shows the V-band polarization position angle of our precessing disk model compared to the observed polarization position angle after correction for interstellar polarization (following the same method as described in Marr et al. 2021). The minimum polarization position angle of our model is ~ 55.8° in 1983, and the maximum is 174.2° in 2021.

Like the Hα EW and V-band photometry, the polarization position angle was also observed to rapidly drop in 2007. Prior to this, our precessing disk model closely follows the observed trend, and fits with a reduced $\chi^2 = 1.4$. After the rapid drop our model is unable to reproduce the observations.
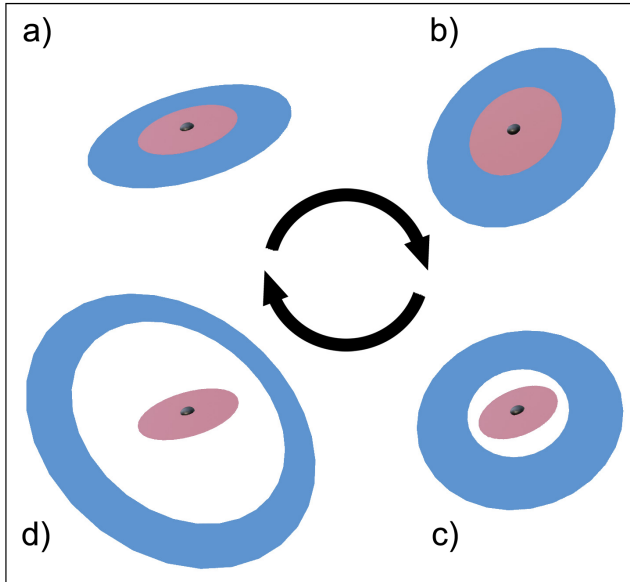
Figure 15. Schematic of the disk tilting and tearing model. The red region of the disk corresponds to the innermost disk, and the blue region corresponds to the outer region which eventually separates. Stage one of our model is represented by a) and b), where the disk is whole and becomes progressively more tilted away from the equator from a) to b). Stage two is represented by c) and d), where the outer region tears, precesses, and eventually dissipates. In stage two, the innermost disk gradually returns to the original inclination at the stellar equator while continuing to build with constant mass injection prior to the cycle repeating. The sizes of the coloured sections are for illustrative purposes only and do not represent actual dimensions.

4.2. *An Ad-hoc Disk Tearing Model*

We find that at some times Pleione's Hα emitting region must be at a different inclination than the V-band emitting region. For example, the precessing disk model shows that while a single disk can reproduce the rapid drop in Hα EW in 2007, the V-band photometry and polarization position angle do not drop at the same time. Based on recent results of Suffak et al. (2022), we propose an ad-hoc model to reproduce the observed trends. These authors investigate the effects that companion stars have on the dynamics of circumstellar disks. They show that in a Be star-binary system with a 30-day orbital period, where the companion is misaligned by 40° from the Be star equatorial plane, the disk can separate into two parts with different inclinations while mass is constantly ejected from the stellar surface. In their simulations, the disk periodically tears and merges back into one disk every 30 orbital periods. While their models consider different mass-loss rates, they find that disk tearing only occurs in active phases, i.e., when mass-loss is on. Their results also suggest that disk tearing can oc-

cur in a variety of different Be star-binary systems with different masses or orbital periods. Previously, a similar phenomenon was modelled in protoplanetary disks of triple-star systems by Kraus et al. (2020), who showed the disk around the primary can break into multiple precessing rings aligned with the companion's orbital planes.

We define our ad-hoc model with two distinct stages which occur in each cycle from a Be-shell phase to Be phase and back. Figure 15 illustrates these stages, with a) and b) corresponding to the first stage, and c) and d) to the second stage. In essence, the first stage is a single disk model which tilts off-axis, and the second stage is a two-disk model with one disk anchored to the stellar equator while the other disk is free to precess.

In the first stage, the disk is whole and fixed to the stellar equator. Owing to the companion's tidal torque, it becomes tilted away from the midplane by $i \approx 30°$ (this tilting has also been shown to occur in the simulations of Suffak et al. 2022 and previously by Cyr et al. 2017). Therefore, in this phase the Hα emitting region – which corresponds to the entire disk, see Carciofi (2011) – and the inner disk – where the V-band flux excess and the optical polarimetry originate – are approximately aligned.

The second stage begins when the disk is torn into two parts. Now, as shown by the simulations of Suffak et al. (2022) and previously outlined by Okazaki (2017), a gap appears between the small inner disk, which is still anchored to the star, and the outer disk, which starts precessing. Therefore, in this phase the Hα emitting region has an orientation that gradually varies in time. Because in this phase the outer disk is no longer fed by the star, it gradually dissipates as the inner disk grows. As a result, the disk slowly transitions to the configuration of the first stage.

The right side of Figure 14 illustrates our ad-hoc model in detail. In the first stage of our model (indicated by dotted lines in the right panel of Figure 14), the innermost disk and Hα emitting region have the same inclination as they gradually change from 60° to 30°. The disk tearing events (1938, 1972, 2007) correspond to the phases immediately before the vertical lines in the figure and mark the beginning of the second stage. Observationally, this stage is related to the Be-shell phase, as the outer disk, now detached from the inner disk, starts precessing around the star. The innermost disk is rebuilt at the original inclination of 60° over $\sim$ 1.5 years, with constant mass-injection during this period as suggested from our Hα modelling in Subsection 4.1. The Hα emitting region begins to precess from 30° to 90°, with a period of $\sim$ 80.5 years following our best-

fit precession model. The precession of the Hα region becomes unstable after ∼ 15 years, and the outer disk then gradually dissipates as gas is lost to the interstellar medium or recombines with the innermost disk. As the inner disk grows, it slowly tilts back to $i \approx 30°$. This marks the phase of the first stage again.

It is important to stress that this ad-hoc model of Pleione's disk addresses the most important observational features seen in the right side of Figure 14, namely

- In the first stage, the gradual change in inclination from 60° to 30° of the inner disk explains the rate of change in brightness, the drop in polarization level and the change in the polarization position angle qualitatively.

- Likewise, the sudden change in the inner disk orientation from 60° to 30° once disk tearing has occurred (during the transition from the first stage to the second) also explains the sudden drop in V-band brightness well, and the dramatic change in the polarization position angle (from ∼ 120° in 2007 to ∼ 50° in 2010).

- The precession model developed in Section 4.1 remains valid, as in the beginning of the second stage (e.g., the shaded area in the right side of Figure 14) the outer disk is allowed to freely precess with a period of 80.5 yrs.

Our ad hoc model, however, is unable to reproduce the strong increase in Hα EW seen in the second half of the first stage (e.g., between 1990 and 2007 in the right side of Figure 14). At this stage the disk becomes gradually more tilted away from the equator and likely also warped (Suffak et al. 2022). The increase in Hα EW might be due to the upper part of the disk, which is closest to the hot stellar poles, becoming hotter and more ionized. This effect, if relevant, is not captured by our simple models that consider axisymmetric and flat disks.

Furthermore, since the density of our disk model was determined solely through Hα line profile fitting, the disk density distribution remains constant through the disk tearing period. Perhaps with this scenario, disk gas could be redistributed within the disk which may alter the value of n at particular snapshots in time at certain radial distances from the central star.

In the models of Suffak et al. (2022), the disk tearing events happen every ∼ 30 orbital cycles for a model with an equal-mass binary in a 30 day orbit. Since Pleione's less massive companion has a 218 day orbital period, this means that more than 57 orbital periods occur before disk tearing every ∼ 34 years.

5. DISCUSSION AND CONCLUSIONS

We began our work by modelling the large-scale structure of Pleione's disk constrained by Hα spectroscopy acquired between 2005 to 2019. During this time, the Hα emission shows that Pleione underwent a transition from a Be phase to a Be-shell phase. We find that one single disk model, with fixed density and size, can reproduce the Hα observations from the above period by simply varying the disk inclination from 30° to 80° at a rate of ∼ 3.7°/year. This best-fit disk model is axisymmetric with a base density of $\rho_0 = 3 \times 10^{-11}$ g cm^{-3}, density power-law exponent of $n = 2.7$, and a minimum outer disk radius of $R_{out} = 15$ R$_{eq}$.

Our Hα disk size agrees with Nemravová et al. (2010) who found that an upper limit on Pleione's outer disk radius is set by the periastron separation of 53 R$_\odot$ (12.1 R$_{eq}$ using the value of R_{eq} in Table 4). However, the outer dimensions of the disk could be restricted by the companion's Roche radius. We note that the lower limit on the outer disk radius, if it is set by the Roche radius, is ∼ 7 R$_{eq}$. We note that in the SPH simulations reported by Cyr et al. (2017), they show in tables 3 and 4 that the truncation radius is larger in systems where the disk and companion's orbital plane are not aligned. A full dynamic simulation will be required to determine whether the disk could be further truncated by the companion's Roche lobe.

We fit a precessing disk model to the inclinations determined through Hα fitting, and find the best-fit model has a minimum inclination of 25°, a maximum inclination of 145°, and a period of ∼ 80.5 years. We extrapolated this model over 120 years to evaluate the fit to archival observations.

We find that this model reproduces the observed EW from 2001 to 2021, including the rapid drop in brightness in 2007. Our model's peak Hα EW is ∼ −2.8 Å while the maximum observed value is ∼ −3.8 Å in ∼ 1960 and again in ∼ 1997. The observed data from ∼ 1970 to ∼ 1985 could also be matched if the precessing model were shifted by ∼ 8 years, so that $i = 30°$ in 1971.

Our precessing model is unable to follow the gradual rise in Hα EW from ∼ 1980 to ∼ 1995 leading to the peak value, and the decrease from ∼ 1997 to ∼ 2001. The V-band magnitude matches from ∼ 1945 to ∼ 1970 and again from ∼ 1990 to ∼ 2007, but fits poorly outside of these times because of the rapid drops in 1971 and 2007. Before 1938 Pleione was diskless, so the model is not expected to reproduce the observed trend before then. The V-band polarization position angle fits from ∼ 1974 to ∼ 2005, and like the V-band magnitude is unable to capture the rapid drop in 2007. We note that the model would reproduce the data if it were to reset

to $i = 60°$ in 2007. We also find the V-band percent polarization fits the observations at all times, but the degree of variation is relatively small.

To align the precessing disk model's polarization position angle to observations, we find that the precession axis of the star must lie at 115° east of north when projected onto the sky. This is in approximate agreement with the value of $\sim 122°$ determined by Hirata (2007) with their model based on observations of the polarization position angle.

We further compared our observed polarization position angles to the interferometric disk normal position angle inferred from interferometric observations. Our values were consistent with those of Touhami et al. (2013) who found a value equivalent to 69° in 2008, and with Cochetti et al. (2019) who found a value equivalent to 63° in 2014 (recall the red dots in the bottom left and right panels of Figure 14).

Overall, the precessing model (in which the whole disk precesses with the same rate and orientation) failed to address most of Pleione's observational features.

Inspired by the recent models of Kraus et al. (2020) and Suffak et al. (2022), we created an ad-hoc disk tearing model which incorporates our precessing disk model and explains the large-scale variations of Pleione's observables, and also seemlessly incorporates the results of Hirata (2007), Tanaka et al. (2007) and Nemravová et al. (2010). In our ad-hoc model, the disk initially is whole and tilted away from the stellar equator. At some point (likely once the disk becomes sufficiently massive), the disk is torn into two parts: an inner part still anchored to the star, having therefore an inclination angle of 60°, and an outer part which is free to precess around the star. What follows is a slow increase in size and density of the inner disk and a gradual dissipation of the outer disk, which is no longer fed by the central star.

Previously, Hirata (2007) and Tanaka et al. (2007) also found that Pleione's disk inclination changes over time. Using a precessing disk model, Hirata (2007) reproduced the change in polarization position angle across the Be-shell to Be transition in 1989. Using the times between edge-on events, they also found the period of precession to be 80.5 years, the same value we determined. Building on Hirata (2007)'s model, Tanaka et al. (2007) claimed that the precessing disk had partially re-accreted leading to the rapid drop in brightness in 2007. They also proposed that the sudden appearance of shell lines alongside the drop could be explained by a secondary disk forming in the stellar equatorial plane, which is consistent with our ad-hoc disk tearing model. Nemravová et al. (2010) also explained the appearance

of shell lines with the formation of a new disk, and we expand on this below.

Our best-fit disk model shows that during the Be to Be-shell transition, that shell lines appear at inclinations near 40° and greater. We acknowledge that these inclinations are smaller than typically assumed for the appearance of Hα shell lines. Hanuschik (1996) studied the geometry of Be star disks including the range of inclinations typical for shell lines. They find that shell lines most frequently occur for disk inclinations of $75° \pm 5°$. However, they focused only on changes in geometry and did not consider disk temperature and the associated changes in ionization fraction nor did they consider the density law. Our best-fit model has a disk density slope of $n = 2.7$, meaning that the density falls more gradually with increasing radius, allowing for shell lines to appear at lower inclinations. Also, viscous disks flare with radial distance from the central star (see, e.g., Carciofi 2011) resulting in more material further from the equatorial plane with increasing radial distance. Silaj et al. (2014) also showed that shell lines could form at lower inclinations. For example, for the B8 Ve star, 4 Aql, they modelled shell lines at inclinations of 46° with $n = 2.5$, and at 43° with $n = 3.0$ and 3.5. Furthermore, in Pleione's tilted disk, the path length through the disk along the line of sight changes over time as the disk inclination varies as well. We also believe that the disk may be warped which could also affect shape of the emission lines although our models only include tilted disks and not warped disks.

We see that when the disk is aligned at the stellar inclination of $61 \pm 9°$, the model agrees with each of the observables, suggesting that our disk model is well constrained. Hirata (2007) noted that at the onset of a shell phase in 1973, the disk's inclination was known to be 60° through polarimetric means. From this, they inferred the star's inclination is also 60°.

We find that our ad-hoc disk tearing model largely reproduces the observed trends of Pleione's circumstellar environment, and agrees with previous descriptions of the disk from the literature. Some details of our model should be examined in further detail, such as the changing thermal structure with a tilting disk, and the dynamical evolution of the disk considering the companion's influence. We also noted a number of other minor discrepancies with work in the literature that we now discuss.

While our model reproduces observations by changing inclination only, we see that small changes to the physical parameters and geometry may help the disk model fit the observables better. In particular, our model suffers from the drawback that the disk is axisymmetric

and flat, while the geometry of a precessing disk is more likely curved or warped, with possible density enhancements (Martin et al. 2009). Because of this, we did not attempt to reproduce the excess Hα flux at high velocities (> 180 km/s) observed from 2006 December to 2007 February. These bumps (recall the middle panel in Figure 9), which were also noted by Nemravová et al. (2010), cause an increase in the EW of the line in the transition to the Be-shell phase. At this time, there is a clear transition where the core of the profile decreases while the flux in the wings of the profile increases. This is strongly indicative of a new disk forming at the equator of the star, while at larger radii the disk continues to dissipate. We expect a fully dynamical computation following our ad-hoc disk tearing model would reproduce these features, as after the disk tears the inner disk would continue to contribute to the high-velocity component of the Hα line profile.

Silaj et al. (2014) modelled Pleione's disk using the same 2007 Dec 18 Hα observation used in this work, and found the disk's density to be $\rho_0 = 6.2 \times 10^{-12}$ g cm^{-3} and $n = 2.5$, at an inclination of 76°. However, we note that our fit is constrained by a series of Hα observations and confirmed by V-band photometric and polarimetric observations which show a clear trend, providing a stronger constraint (Klement et al. 2015).

Pleione is presently in a Be-shell phase which began in 2007. As the inclination of the Hα emitting region is once again nearly edge-on, this marks the half-way point to the next rapid drop in brightness. We highly encourage astronomers to continue collecting high time-resolution data on this unique system, to motivate not only the study of Pleione, but other Be stars, such as γ Cas and 59 Cyg (Hummel 1998), that have been found to have variable disk inclinations. In addition to studying the large-scale variations caused by the influence of companions on the disk, the impact of smaller scale dynamical changes on the disk, such as those found by Wang et al. (2017), should be investigated as well. Future work should also investigate whether SPH simulations using Pleione's orbital parameters are able to explain both the disk tearing period and the outer disk precession period. In our follow-up work, we will determine the effect of disk tilting on the thermal structure of Pleione's disk.

REFERENCES

Abt, H. A., & Levato, H. 1978, PASP, 90, 201, doi: 10.1086/130308

Auer, L. H., & Mihalas, D. 1968, ApJ, 153, 245, doi: 10.1086/149654

Binnendijk, L. 1949, AJ, 54, 117, doi: 10.1086/106209

Boehme, D. 1988, Information Bulletin on Variable Stars, 3222, 1

Bohme, D. 1984, Information Bulletin on Variable Stars, 2507, 1

—. 1985, Information Bulletin on Variable Stars, 2723, 1

—. 1986, Information Bulletin on Variable Stars, 2893, 1

Carciofi, A. C. 2011, in Active OB Stars: Structure, Evolution, Mass Loss, and Critical Limits, ed. C. Neiner, G. Wade, G. Meynet, & G. Peters, Vol. 272, 325–336, doi: 10.1017/S1743921311010738

Carciofi, A. C., & Bjorkman, J. E. 2006, ApJ, 639, 1081, doi: 10.1086/499483

Carciofi, A. C., Magalhães, A. M., Leister, N. V., Bjorkman, J. E., & Levenhagen, R. S. 2007, ApJL, 671, L49, doi: 10.1086/524772

Cochetti, Y. R., Arcos, C., Kanaan, S., et al. 2019, A&A, 621, A123, doi: 10.1051/0004-6361/201833551

Cox, A. N. 2000, Allen's astrophysical quantities (New York: AIP Press; Springer)

Cyr, I. H., Jones, C. E., Panoglou, D., Carciofi, A. C., & Okazaki, A. T. 2017, MNRAS, 471, 596, doi: 10.1093/mnras/stx1427

Dapergolas, A., di Cola, G., Guarnieri, A., & Madama, G. 1981, Information Bulletin on Variable Stars, 1920, 1

Delplace, A.-M., & Hubert, H. 1973, Academie des Sciences Paris Comptes Rendus Serie B Sciences Physiques, 277, 575

Doazan, V., & Underhill, A. 1986, B Stars With and Without Emission Lines (National Aeronautics and Space Administration)

Draper, Z. H., Wisniewski, J. P., Bjorkman, K. S., et al. 2014, ApJ, 786, 120, doi: 10.1088/0004-637X/786/2/120

Ducati, J. R. 2002, VizieR Online Data Catalog

Dunn, R. J. H., Fabian, A. C., & Sanders, J. S. 2006, MNRAS, 366, 758, doi: 10.1111/j.1365-2966.2005.09928.x

Egan, M. P., Price, S. D., Kraemer, K. E., et al. 2003, VizieR Online Data Catalog, V/114

ESA. 2000, INES 3.0 Search Output Description. http://sdc.cab.inta-csic.es/ines/OutForm.html

Fitzpatrick, E. L. 1999, PASP, 111, 63, doi: 10.1086/316293

Foreman-Mackey, D., Hogg, D. W., Lang, D., & Goodman, J. 2013, PASP, 125, 306, doi: 10.1086/670067

Freire Ferrero, R., Morales Durán, C., Halbwachs, J.-L., & Cabo Cubeiro, A. M. 2012, AJ, 143, 28, doi: 10.1088/0004-6256/143/2/28

Frémat, Y., Zorec, J., Hubert, A.-M., & Floquet, M. 2005, A&A, 440, 305, doi: 10.1051/0004-6361:20042229

Frost, E. B. 1906, ApJ, 23, doi: 10.1086/141340

Frost, E. B., Barrett, S. B., & Struve, O. 1926, ApJ, 64, 1, doi: 10.1086/142986

Gaia Collaboration, Brown, A. G. A., Vallenari, A., et al. 2020, Gaia Early Data Release 3: Summary of the contents and survey properties. https://arxiv.org/abs/2012.01533

Georgy, C., Ekström, S., Granada, A., et al. 2013, A&A, 553, A24, doi: 10.1051/0004-6361/201220558

Gies, D. R., McKibben, W. P., Kelton, P. W., Opal, C. B., & Sawyer, S. 1990, AJ, 100, 1601, doi: 10.1086/115620

González-Riestra, R., Solano, E., Talavera, A., et al. 2001, in Astronomical Society of the Pacific Conference Series, Vol. 238, Astronomical Data Analysis Software and Systems X, ed. J. Harnden, F. R., F. A. Primini, & H. E. Payne, 156

Gulliver, A. F. 1977, ApJS, 35, 441, doi: 10.1086/190487

Hall, J. C., Fulton, E. E., Huenemoerder, D. P., Welty, A. D., & Neff, J. E. 1994, PASP, 106, 315, doi: 10.1086/133381

Hall, J. C., & Lockwood, G. W. 1995, ApJ, 438, 404, doi: 10.1086/175084

Hanuschik, R. W. 1996, A&A, 308, 170

Hirata, R. 1995, PASJ, 47, 195

Hirata, R. 2007, in Astronomical Society of the Pacific Conference Series, Vol. 361, Active OB-Stars: Laboratories for Stellare and Circumstellar Physics, ed. A. T. Okazaki, S. P. Owocki, & S. Stefl, 267

Hirata, R., & Kogure, T. 1976, PASJ, 28, 509

—. 1977, PASJ, 29, 477

Hopp, U., & Witzigmann, S. 1980, Information Bulletin on Variable Stars, 1782

Hopp, U., Witzigmann, S., & Geyer, E. H. 1982, Information Bulletin on Variable Stars, 2148

Hummel, W. 1998, A&A, 330, 243

Iliev, L. 2019, IAU Symposium, 346, 149, doi: 10.1017/S1743921319002345

Iliev, L., Koubský, P., Kubát, J., & Kawka, A. 2007, in Astronomical Society of the Pacific Conference Series, Vol. 361, Active OB-Stars: Laboratories for Stellare and Circumstellar Physics, ed. A. T. Okazaki, S. P. Owocki, & S. Stefl, 440

Katahira, J.-I., Hirata, R., Ito, M., et al. 1996a, PASJ, 48, 317, doi: 10.1093/pasj/48.2.317

Katahira, J.-I., Hirata, R., Ito, M., et al. 1996b, in Revista Mexicana de Astronomia y Astrofisica Conference Series, Vol. 5, Revista Mexicana de Astronomia y Astrofisica Conference Series, ed. V. Niemela, N. Morrell, P. Pismis, & S. Torres-Peimbert, 114

Klement, R., Carciofi, A. C., Rivinius, T., et al. 2015, A&A, 584, A85, doi: 10.1051/0004-6361/201526535

Kraus, S., Kreplin, A., Young, A. K., et al. 2020, Science, 369, 1233, doi: 10.1126/science.aba4633

Lindblad, B. 1922, ApJ, 55, 85, doi: 10.1086/142660

Magalhaes, A. M., Benedetti, E., & Roland, E. H. 1984, PASP, 96, 383, doi: 10.1086/131351

Magalhaes, A. M., Rodrigues, C. V., Margoniner, V. E., Pereyra, A., & Heathcote, S. 1996, in Astronomical Society of the Pacific Conference Series, Vol. 97, Polarimetry of the Interstellar Medium, ed. W. G. Roberge & D. C. B. Whittet, 118

Marr, K. C., Jones, C. E., Carciofi, A. C., et al. 2021, arXiv e-prints, arXiv:2103.06948. https://arxiv.org/abs/2103.06948

Marr, K. C., Jones, C. E., & Halonen, R. J. 2018, ApJ, 852, 103, doi: 10.3847/1538-4357/aaa0d0

Martin, R. G., Pringle, J. E., & Tout, C. A. 2009, MNRAS, 400, 383, doi: 10.1111/j.1365-2966.2009.15465.x

Martin, R. G., Pringle, J. E., Tout, C. A., & Lubow, S. H. 2011, MNRAS, 416, 2827, doi: 10.1111/j.1365-2966.2011.19231.x

McLaughlin, D. B. 1938, ApJ, 88, 622, doi: 10.1086/144014

Merrill, P. W., & Burwell, C. G. 1933, ApJ, 78, 87, doi: 10.1086/143490

Mota, B. C. 2019, PhD thesis, University of São Paulo, doi: 10.11606/T.14.2020.tde-26052019-143801

Moultaka, J., Ilovaisky, S. A., Prugniel, P., & Soubiran, C. 2004, PASP, 116, 693, doi: 10.1086/422177

Murakami, H., Baba, H., Barthel, P., et al. 2007, Publications of the Astronomical Society of Japan, 59, S369, doi: 10.1093/pasj/59.sp2.S369

Nemravová, J., Harmanec, P., Kubát, J., et al. 2010, A&A, 516, A80, doi: 10.1051/0004-6361/200913885

Neugebauer, G., Habing, H. J., van Duinen, R., et al. 1984, ApJL, 278, L1, doi: 10.1086/184209

Okazaki, A. T. 2017, in The Lives and Death-Throes of Massive Stars, ed. J. J. Eldridge, J. C. Bray, L. A. S. McClelland, & L. Xiao, Vol. 329, 432–432, doi: 10.1017/S1743921317003143

Parsons, H. M. 1918, ApJ, 47, 38, doi: 10.1086/142378

Poeckert, R., & Marlborough, J. M. 1979, ApJ, 233, 259, doi: 10.1086/157387

Pojmanski, G. 1997, AcA, 47, 467. https://arxiv.org/abs/astro-ph/9712146

Pollmann, E. 2011, BAV Rundbrief - Mitteilungsblatt der Berliner Arbeits-gemeinschaft fuer Veraenderliche Sterne, 60, 5

—. 2020, BAV Rundbrief - Mitteilungsblatt der Berliner Arbeits-gemeinschaft fuer Veraenderliche Sterne, 69, 81

Rivinius, T., Carciofi, A. C., & Martayan, C. 2013, A&A Rv, 21, 69, doi: 10.1007/s00159-013-0069-0

Rohatgi, A. 2020, Webplotdigitizer: Version 4.4. https://automeris.io/WebPlotDigitizer

Sharov, A. S., & Lyutyi, V. M. 1988, Soviet Ast., 32, 303

—. 1992, Soviet Ast., 36, 275

—. 1997, Astronomy Letters, 23, 93

Silaj, J., Jones, C. E., Sigut, T. A. A., & Tycner, C. 2014, ApJ, 795, 82, doi: 10.1088/0004-637X/795/1/82

Skrutskie, M. F., Cutri, R. M., Stiening, R., et al. 2006, AJ, 131, 1163, doi: 10.1086/498708

Stauffer, J. R., Hartmann, L. W., Fazio, G. G., et al. 2007, ApJS, 172, 663, doi: 10.1086/518961

Suffak, M., Jones, C. E., & Carciofi, A. C. 2022, MNRAS, 509, 931, doi: 10.1093/mnras/stab3024

Tanaka, K., Sadakane, K., Narusawa, S.-Y., et al. 2007, PASJ, 59, L35, doi: 10.1093/pasj/59.4.L35

Touhami, Y., Gies, D. R., Schaefer, G. H., et al. 2013, ApJ, 768, 128, doi: 10.1088/0004-637X/768/2/128

van Leeuwen, F. 2007, A&A, 474, 653, doi: 10.1051/0004-6361:20078357

Wang, L., Gies, D. R., & Peters, G. J. 2017, ApJ, 843, 60, doi: 10.3847/1538-4357/aa740a

Werner, M. W., Roellig, T. L., Low, F. J., et al. 2004, ApJS, 154, 1, doi: 10.1086/422992

Wright, E. L., Eisenhardt, P. R. M., Mainzer, A. K., et al. 2010, AJ, 140, 1868, doi: 10.1088/0004-6256/140/6/1868